SUB-RADIANCE AND ENHANCED-RADIANCE OF UNDULATOR RADIATION FROM A CORRELATED ELECTRON BEAM*

R. Ianconescu, University of Tel-Aviv, Tel-Aviv and Shenkar College, Ramat Gan, Israel
E. Hemsing, A. Marinelli, SLAC, Menlo Park, California, USA
A. Nause, UCLA, Los Angeles, USA
A. Gover, University of Tel-Aviv, Tel-Aviv, Israel

Abstract

The radiant intensity of Synchrotron Undulator Radiation (UR) depends on the current noise spectrum of the electron beam injected into the wiggler. The current noise spectrum and intensity can be controlled (suppressed or enhanced relative to the shot-noise level) by the effect of collective longitudinal space charge interaction in drift and dispersion sections [1]. This new control lever is of significant interest for possible control of SASE in FEL, since UR is the incoherent seed of SASE. Thus, control of spontaneous UR is a way to enhance the coherence of seeded FEL [2, 3], or alternatively, obtain enhanced radiation from a cascade noise-amplified electron beam [4]. The dependence of UR emission on the current noise is primarily a result of the longitudinal correlation of the e-beam distribution due to the longitudinal space charge effect. However, at short wavelengths, 3-D effects of transverse correlation and effects of emittance disrupt the proportionality relation between the UR intensity and e-beam current noise. We present analysis and simulation of UR sub-radiance/enhanced-radiance under various ranges of beam parameters, and compare to recent experimental observations [1].

INTRODUCTION

This study is an extension of previous work on current noise correlation effects due to longitudinal space charge (LSC) interactions effects in a drifting electron beam, such as microbunching instability [5] and e-beam noise suppression effects [6–14] which are of particular interest at the short wavelength limit [15] where it may be relevant for coherence enhancement of XUV FELs. The understanding and control of UR from a correlated electron beam is of major interest because UR is an important source of radiation for applications, and it is the start radiation field of SASE FEL. UR can be also an efficient diagnostic mean for evaluating e-beam current noise in a wide range of the spectrum, especially because it emits radiation on axis (contrary to OTR diagnostics). 3D correlation effects on UR that have been observed experimentally [1] have received little attention so far. The model presented in this paper is intended for study of such 3D effects.

SPONTANEOUS RADIATION EMISSION FROM FREE ELECTRONS

The radiation mode expansion analysis of superradiant emission from particulate current in [16] can be extended to analysis of radiation into plane waves from any free electron radiation source in the far field zone. This results in a dipole antenna expression for the spectral radiant intensity

$$\frac{d^2\breve{W}}{d\omega d\Omega} = \frac{\eta_0 k^2}{16\pi^3}|\breve{\underline{d}}|^2 \sin^2\psi, \tag{1}$$

where

$$\breve{\underline{d}}(\omega,\underline{k}) \equiv \sum_j \Delta\breve{\underline{d}}_j, \tag{2}$$

$$\Delta\breve{\underline{d}}_j \equiv -e\int_{-\infty}^{\infty} dt \underline{v}_j(t) e^{i\omega t - i\underline{k}\cdot\underline{r}_j(t)}, \tag{3}$$

and

$$\underline{k} = k(\hat{e}_x \sin\Theta_x + \hat{e}_y \sin\Theta_y + \hat{e}_z \cos\Theta) \tag{4}$$

SPONTANEOUS EMISSION FROM A CORRELATED ELECTRON BEAM

Here we extend the radiation mode expansion formulation of [16] for superradiance and stimulated superradiance from an electron beam to the case of emission from a correlated or uncorrelated electron beam into plane waves in the far field. This includes the cases of a randomized (Poisson distribution) electron beam producing conventional incoherent spontaneous emission, a prebunched beam producing superradiant emission, a random beam of super-Poissonian distribution producing enhanced radiance spontaneous emission or a beam of sub-Poissonian distribution that produces sub-radiance (suppressed spontaneous emission). So far, the formulation is valid for general radiation schemes of free electrons. In the next section we specify to the case of undulator radiation.

For spontaneous emission, the system is stationary in the sense that it is not sensitive to the absolute time of the interaction. Defining t_{0j} the time electron j enters the interaction region, $\Delta\breve{\underline{d}}_j$ in Eq. (3) is written as

$$\Delta\breve{\underline{d}}_j = -e\int_{t_{0j}}^{t_j(L)} dt \underline{v}_j^{(0)}(t-t_{0j}) e^{i\omega t - i\underline{k}\cdot\underline{r}_j^{(0)}(t-t_{0j})}, \tag{5}$$

and we set the integration limits from the entering time t_{0j} to the exit time $t_j(L)$, L being the interaction length. By changing variable $t' = t - t_{0j}$, we obtain

$$\Delta\breve{\underline{d}}_j = \Delta\breve{\underline{d}}_j^{(0)} e^{i\omega t_{0j}} \tag{6}$$

where

$$\Delta\breve{\underline{d}}_j^{(0)} = -e\int_0^{\Delta t_j(L)} dt' \underline{v}_j^{(0)}(t') e^{i\omega t' - i\underline{k}\cdot\underline{r}_j^{(0)}(t')}. \tag{7}$$

* This research was supported in part by a grant from the United States-Israel Binational Science Foundation(BSF), Jerusalem, ISRAEL

ISBN 978-3-95450-134-2

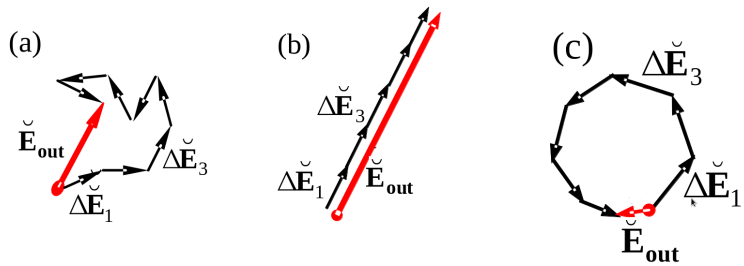

Figure 1: Different cases of e-beam correlations, showing how the fields add for each. Panel (a) shows an uncorrelated beam and fields add according to "random walk". Panel (b) shows full superradiance, in which case all the fields add with the same phase and panel (c) shows full subradiance in which case the electrons are anti-correlated and the radiation sums to something close to 0.

The upper limit $\Delta t_j(L) \equiv t_j(L) - t_{0j}$ depends on the trajectory of the electron, but is independent of the entering time t_{0j}. Setting Eqs. (2) and (6) into (1), we obtain

$$\frac{d^2\breve{W}}{d\omega d\Omega} = \frac{\eta_0 k^2}{16\pi^3}\sin^2\psi\left|\sum_j \Delta\breve{d}_j^{(0)} e^{i\omega t_{0j}}\right|^2. \tag{8}$$

This result can be averaged over the transverse statistics of electron trajectories, and over the longitudinal distribution statistics of the arrival times t_{0j}: $\langle\rangle$ means averaging over an ensemble of different realizations (different electron beam pulses). Putting the averaging inside the sums we obtain

$$\left\langle\frac{d^2\breve{W}}{d\omega d\Omega}\right\rangle = \frac{\eta_0 k^2}{16\pi^3}\sin^2\psi\left[\sum_j\left\langle\left|\Delta\breve{d}_j^{(0)}\right|^2\right\rangle + \sum_{j\neq k}\left\langle\Delta\breve{d}_j^{(0)}\Delta\breve{d}_k^{(0)*}e^{i\omega(t_{0j}-t_{0k})}\right\rangle\right]. \tag{9}$$

Considering that $\breve{d}^{(0j)}$ is independent of t_{0j} (see Eq. (6)) the averaging over the ensemble of realizations can be split into averaging over t_{0j} and averaging over the other trajectory parameters $(\underline{r}_{\perp 0j}, \underline{\beta}_{0j})$.

$$\left\langle\frac{d^2\breve{W}}{d\omega d\Omega}\right\rangle = \frac{\eta_0 k^2}{16\pi^3}\sin^2\psi\left[\left\langle\sum_j\left|\Delta\breve{d}_j^{(0)}\right|^2\right\rangle + \sum_{j\neq k}\left\langle\Delta\breve{d}_j^{(0)}\Delta\breve{d}_k^{(0)*}\right\rangle\left\langle e^{i\omega(t_{0j}-t_{0k})}\right\rangle\right]. \tag{10}$$

Often the transverse correlation effect between the electrons is neglected (in particular in the case of a narrow electron beam [17, 18]) and then (and only then) $\left\langle\Delta\breve{d}_j^{(0)}\Delta\breve{d}_k^{(0)*}\right\rangle = \left\langle\Delta\breve{d}_j^{(0)}\right\rangle\left\langle\Delta\breve{d}_k^{(0)*}\right\rangle = \left\langle\left|\Delta\breve{d}_j^{(0)}\right|^2\right\rangle$, and one obtains the 1D case result:

$$\left\langle\frac{d^2\breve{W}}{d\omega d\Omega}\right\rangle = \frac{\eta_0 k^2}{16\pi^3}\sin^2\psi\left\langle\left|\Delta\breve{d}^{(0)}\right|^2\right\rangle\left[N + \sum_{j\neq k}\left\langle e^{i\omega(t_{0j}-t_{0k})}\right\rangle\right]. \tag{11}$$

where $\langle|\Delta\breve{d}^{(0)}|^2\rangle$ is an average over the trajectories $(\underline{r}_{\perp 0j}, \underline{\beta}_{0j})$. In case of a random beam (shot-noise), the arrival times of each pair of electrons are independent, and one may again decompose $\left\langle e^{i\omega(t_{0j}-t_{0k})}\right\rangle = \left\langle e^{i\omega t_{0j}}\right\rangle\left\langle e^{-i\omega t_{0k}}\right\rangle$ and each individual term is 0, resulting in

$$\left\langle\frac{d^2\breve{W}}{d\omega d\Omega}\right\rangle\Big|_{shot} = \frac{\eta_0 k^2}{16\pi^3}\sin^2\psi\left\langle\left|\Delta\breve{d}^{(0)}\right|^2\right\rangle N, \tag{12}$$

which is the expression for the spectral radiant energy intensity of conventional spontaneous radiation emission produced by the "shot-noise" of an uncorrelated electron beam. This case happens if:

$$\left\langle e^{i\omega(t_{0j}-t_{0k})}\right\rangle = 0, \tag{13}$$

As is evident from Eq. (11) there is enhanced radiant emission if the beam is correlated such that:

$$\left\langle e^{i\omega(t_{0j}-t_{0k})}\right\rangle > 0, \tag{14}$$

and there is subradiance if the beam electrons are anti-correlated:

$$\left\langle e^{i\omega(t_{0j}-t_{0k})}\right\rangle < 0. \tag{15}$$

Full superradiance occurs when all arrival times are identical, so that $t_{0j} = t_{0k}$ (maximum bunching). In such a case $\left\langle e^{i\omega(t_{0j}-t_{0k})}\right\rangle = 1$, and Eq. (11) results in

$$\left\langle\frac{d^2\breve{W}}{d\omega d\Omega}\right\rangle = \frac{\eta_0 k^2}{16\pi^3}\sin^2\psi\left\langle\left|\Delta\underline{\breve{d}}^{(0)}\right|^2\right\rangle N^2 = N\left\langle\frac{d^2\breve{W}}{d\omega d\Omega}\right\rangle\Big|_{shot}, \tag{16}$$

Superradiance occurs also if the e-beam is periodically bunched (see [16]). See also [19] in which it is shown an extreme case of subradiance in case the granularity of the current is 0, meaning 0 shot noise.

These different cases of correlated beam radiance are displayed schematically in Figure 1 as a complex field summation of the radiation wavepackets field from the individual electrons.

Note that if one wants to keep 3D effects in the analysis, it is necessary to stay with the exact expression in Eq. (8), as we do in our simulations.

ISBN 978-3-95450-134-2

EXPLICIT EXPRESSION FOR RADIATION FROM A LINEAR UNDULATOR

We consider here a beam in a linear undulator having a known transverse velocity in the $\hat{e}_x$ direction due to the undulator: $v_w = c\beta_w = ca_w/\gamma$, $a_w = eB_w/(mck_w)$ being the "wiggler parameter", $k_w = 2\pi/\lambda_w$ is the undulator wavenumber and B_w is the amplitude of the magnetic field. In addition, there are transverse initial velocities in the $\hat{e}_x$ and $\hat{e}_y$ directions for each electron injected into the undulator at $z = 0$: $\underline{v}_{\perp 0j}$ and initial positions in the $\hat{e}_x$ and $\hat{e}_y$ directions at the undulator entry, which we call $\underline{r}_{\perp 0j}$.

Neglecting now betatron oscillation inside the undulator, the velocity of electron j inside the undulator entering at t_{0j} is

$$\underline{v}_j(t) = \underline{v}_{\perp 0j} + Re[\tilde{\underline{v}}_w e^{-ik_w z_j(t)}] + \hat{e}_z v_{0zj}. \quad (17)$$

We neglect for now the longitudinal quiver ($a_w \ll 1$), so that we assume $v_{zj} = v_{0zj}$ is a constant in z. Hence we use the electron longitudinal velocity averaged over the undulator period:

$$z_j(t) = v_{zj}t, \quad (18)$$

and the transverse position is

$$\underline{r}_{\perp j}(t) = \underline{r}_{\perp j} + \underline{v}_{\perp 0j}t + Re[\tilde{\underline{r}}_w e^{-ik_w z_j(t)}] \quad (19)$$

From the real part in Eq. (17), $\tilde{v}_w e^{-ik_w z_j(t)}$ contributes the forward radiation, while its complex conjugate contributes the backward radiation at Doppler down shifted low frequency. Hence we neglect the complex conjugate. We shall also neglect the transverse quiver in Eq. (19) (which can produce harmonic emission off-axis). Setting Eqs. (18) and (17) into Eq. (7), and changing the integration variable $z = v_{zj}t$ one obtains

$$\Delta\breve{d}_j^{(0)} = -e\frac{\tilde{\beta_w}}{2\beta_{zj}} e^{-i\underline{k}_\perp \cdot \underline{r}_{\perp 0j}} \int_0^L dz e^{i\theta_j z}, \quad (20)$$

which results in

$$\Delta\breve{d}_j^{(0)} = -e\frac{\tilde{\beta_w}}{2\beta_{zj}} e^{-i\underline{k}_\perp \cdot \underline{r}_{\perp 0j}} e^{i\theta_j L/2} L\,\mathrm{sinc}(\theta_j L/2), \quad (21)$$

where

$$\theta_j(\omega) = \omega/v_{zj} - k_z - k_w - \underline{k}_\perp \cdot \beta_{\perp j}/\beta_{zj} \quad (22)$$

is the detuning parameter. So the expression for the radiant spectral energy intensity is obtained from Eq. (8)

$$\frac{d^2\breve{W}}{d\omega d\Omega} = \frac{e^2\eta_0 k^2}{16\pi^3} \sin^2\psi \frac{|\tilde{a}_w|^2 L^2}{4\gamma^2\beta_z^2} \left|\sum_j \mathrm{sinc}(\theta_j L/2) e^{i\theta_j L/2} e^{i\omega t_{0j} - i\underline{k}_\perp \cdot \underline{r}_{\perp 0j}}\right|^2, \quad (23)$$

where the z velocity of the j electron inside the undulator averaged over the longitudinal quiver is given by

$$\beta_{zj}^2 = \beta_j^2 - \beta_w^2/2 - \beta_{0x}^2 - \beta_{0y}^2, \quad (24)$$

and the wiggler velocity square β_w^2 is divided by 2 for the case of linear wiggle. β_j is the total velocity of electron j (or the velocity before entering the wiggler).

RADIANT ENERGY INTENSITY

For small angular spread and small energy spread (cold beam) all θ_j are approximately equal, so one may write the spectral energy radiant intensity as

$$\frac{d^2\breve{W}}{d\omega d\Omega} \simeq \frac{e^2\eta_0 k^2}{16\pi^3} \sin^2\psi \frac{|\tilde{a}_w|^2 L^2}{4\gamma^2\beta_z^2} \mathrm{sinc}^2(\theta L/2) \left|\sum_j e^{i\omega t_{0j} - i\underline{k}_\perp \cdot \underline{r}_{\perp 0j}}\right|^2, \quad (25)$$

and neglecting the velocity spread, θ is approximately

$$\theta \simeq \omega/v_z - k_z - k_w = \omega/v_z - \omega\cos\Theta/c - k_w. \quad (26)$$

The condition $\theta = 0$ defines the center frequency at observation angle Θ:

$$\omega_0 = \frac{ck_w}{1/\beta_z - \cos\Theta}, \quad (27)$$

so θ can be written

$$\theta = k_w \frac{\omega - \omega_0}{\omega_0}. \quad (28)$$

Considering the width of the sinc^2 function, one can define the spectral width $\Delta\omega$ at any observation angle Θ as

$$\frac{\Delta\omega}{\omega_0} = \frac{\lambda_w}{L} = 1/N_w, \quad (29)$$

By direct integration one can show that the total frequency integrated radiant energy intensity is

$$\frac{dW}{d\Omega} = \int_{-\infty}^{\infty} \frac{d^2\breve{W}}{d\omega d\Omega} d\omega = \left.\frac{d^2\breve{W}}{d\omega d\Omega}\right|_{\omega_0} \Delta\omega. \quad (30)$$

For small angular and energy spread the line broadening (29) is the same as in a cold beam limit ("homogeneous broadening"). Using the above in Eq. (23), one gets

$$\frac{dW}{d\Omega} = \frac{e^2\eta_0 k_0^2}{16\pi^3} \sin^2\psi \frac{|\tilde{a}_w|^2 L^2}{4\gamma^2\beta_z^2} \frac{\omega_0}{N_w} \left|\sum_j \mathrm{sinc}(\theta_{j0} L/2) e^{i\theta_{j0} L/2} e^{i\omega_0 t_{0j} - i\underline{k}_{\perp 0} \cdot \underline{r}_{\perp 0j}}\right|^2, \quad (31)$$

where $\omega_0 = \omega_0(\Theta)$ is defined by (27) and θ_{j0}, $\underline{k}_{\perp 0}$ are defined by (22), (4) with $\omega = \omega_0(\Theta)$, $k = \omega_0(\Theta)/c$.

ISBN 978-3-95450-134-2

EXPERIMENTAL OBSERVATIONS AND SIMULATION RESULTS

We have recently demonstrated for the first time control over spontaneous emission of undulator radiation by establishing in the e-beam, prior to injection into the undulator, longitudinal (temporal) correlation between the electrons. This was done in a set-up composed of a drift section (in which longitudinal space charge interaction correlates the velocities of the electrons) and a dispersive section (chicane) that correlates the longitudinal positions (or the injection times t_{0j}) of the electrons [1]. Figure 2 shows the UR radiant intensity on-axis as a function of the chicane compaction parameter R_{56}. The curve is normalized to the UR radiant intensity of an almost uncorrelated beam ($R_{56} = 0$). The experiment shows attainment of up to ×2.6 suppression factor of the UR (sub-radiance) and up to ×2.6 enhancement factor (enhanced-radiance) at higher R_{56}. The experiment was carried out in NLCTA with a 120 MeV, 25 pC beam and a periodic wiggler that generated $\lambda = 800$ nm UR on axis. In the experiment [1] also the UR radiant intensity dependence on off-axis angle Θ was measured for various levels of R_{56}. Figure 2 shows the suppression ratio of the UR dependence on Θ for various values of R_{56} relative to the case of $R_{56} = 0$. The data shows that there is significant UR suppression also at off-axis angles, however the suppression factor deteriorates (gets closer to 1) at larger off-axis angles, especially when the on-axis suppression factor is minimal ($R_{56} \simeq 2$ mm).

Another interesting experimental result is described by the red data points in Fig. 2(b) and 3. They show the deterioration of both the suppression and the enhancement effects (the gain factor relative to an uncorrelated beam gets closer to 1) when a thin foil is placed on the way of the beam before it is injected into the wiggler. It is expected that the angular scattering in the foil diminishes the longitudinal and transverse correlation that was established in the beam prior to injection.

In a 1D model it is expected that the undulator radiation is proportional to the spectral density of the e-beam current (which is the current shot-noise when the beam is uncorrelated). However a 3D model would reveal deviations from such proportionality. In particular it is evident from Eqs. (22) and (31) that the UR emission off-axis would be affected not only by the longitudinal correlation in the beam (t_{0j}) but also by the transverse correlations ($\underline{r}_{\perp 0j}$, $\underline{\beta}_{\perp 0j}$) that develop in the beam drift section. We presume that these 3D effects should explain the experimental results displayed in Figs. 2 and 3. This is the motivation for the analysis and simulations of the correlated beam UR that are presented in this paper.

In order to simulate the UR from a correlated electron beam including 3D effects of transverse e-beam correlation and off-axis radiation emission we use a 3D particle simulation code (GPT) that simulates the electron dynamics in the drift section, including 3D Coulomb interaction between the particles in a finite cross section e-beam [17]. The effect of the dispersive section is taken into consideration us-

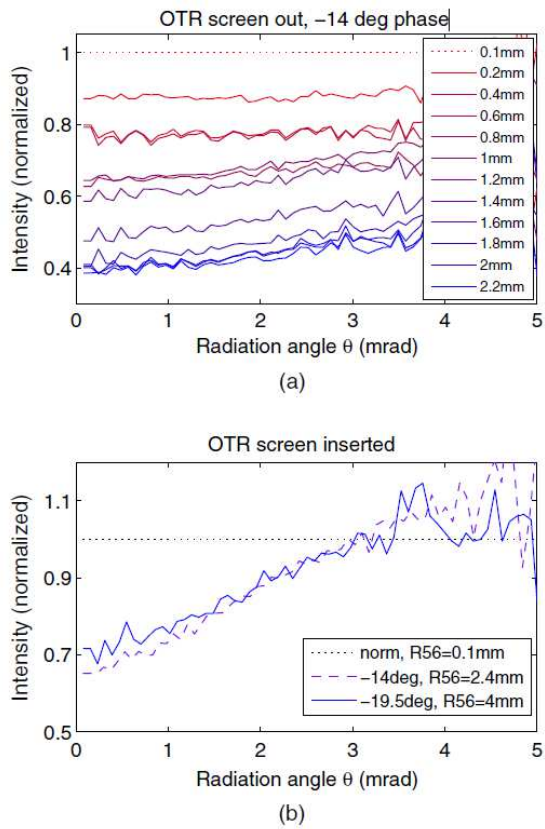

Figure 2: from [1]: Radiation intensity as a function of angle from direction of motion normalized by the measurement with $R_{56} = 0.1$ mm. (a) Case of -14 deg gun phase for different values of R_{56}. Suppression is slightly stronger on axis, but is relatively uniform across the FWHM beam (2 mrad). (b) Inserting an OTR screen increases emittance, which amplifies angular effects. At optimal suppression for both -14 deg and -19 deg gun phases, the degree of suppression is angle dependent, with suppression predominantly on axis. Data for the -14 deg case corresponds to the red square, $R_{56} = 2.4$ mm in Fig. 3.

ing a Matlab program based on the transformation equation $z'_j \rightarrow z_j + R_{56}(\gamma_j - \gamma)/\gamma$. The 6D coordinates of all particles are then used in the Matlab program (based on equations (22) and (23)) as the initial condition parameters ($\underline{\beta}_{0j}$, $\underline{r}_{\perp 0j}$, t_{0j}) needed for the computation of the spectral radiant intensity as function of frequency ω and emission angle Θ. The GPT 3D simulation establishes the longitudinal beam correlation effect and the suppression (or enhancement) of the electron beam shot noise [17]. But it also establishes transverse correlation [18] between the electrons $\underline{r}_{\perp 0j}$ which come into expression in the full 3D model of UR (Eqs. (22) and (23)), especially when we consider off-axis emission and e-beam angular spread. We show in Fig. 4 some initial results of simulation of correlated beam UR. Because of limited computer resources, simulations were not carried out with the same experimental parameters of [1], but for a lower energy beam (100 MeV) that generates on axis with

ISBN 978-3-95450-134-2

the same wiggler parameters a longer wavelength ($\lambda = 2\,\mu m$) instead of 0.8 µm used in [1].

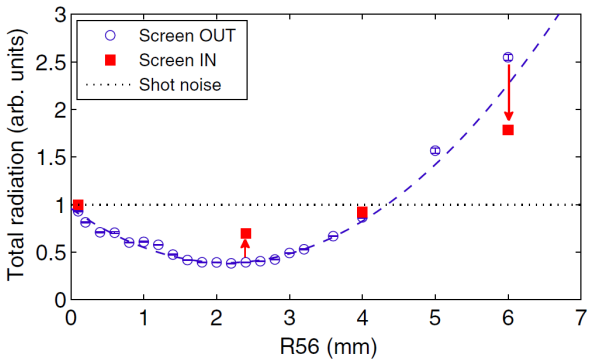

Figure 3: from [1]: Intensity on the camera as a function of chicane R_{56} at -14 deg phase with OTR screen OUT (blue circles) and screen IN (red squares). The dotted black line shows the inferred shot noise level. Insertion of a thin foil on the way of the beam before injection into the wiggler scatters the beam, spoils the correlation, and shifts intensity towards the shot noise level (but does not fully suppress coherent effects).

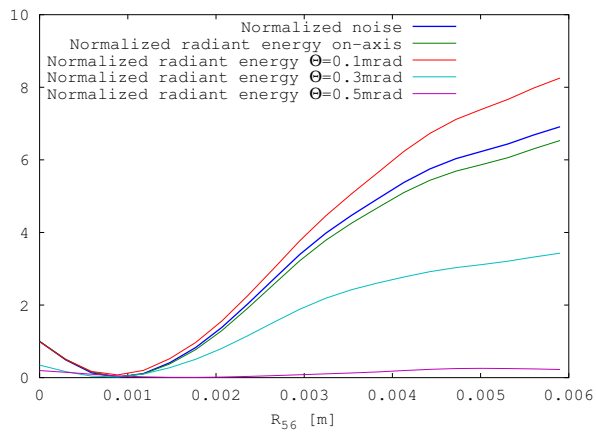

Figure 4: Noise and radiant energy intensity as function of R_{56}. Both the noise and the radiant energy intensity are computed at the center frequency for the same realization, namely the same random initial condition of an injected beam (single pulse). The noise is normalized to its value for $R_{56} = 0$ and the radiant energy intensity is normalized relative to it's value for $R_{56} = 0$, on axis, i.e. $\Theta = 0$. The diagram demonstrates deviation of the correlated beam UR from the current noise for large values of R_{56} and Θ.

In Fig. 5 we show correlated current noise and radiant intensity on axis, as function of frequency, and in Fig. 5b the ratio between them. The ratio of the spectra (Fig. 5b) replicates the ideal sinc^2 dependence. In Fig. 4 noise and radiant energy intensity at different observation angles as function of R_{56}. The figure shows good proportionality

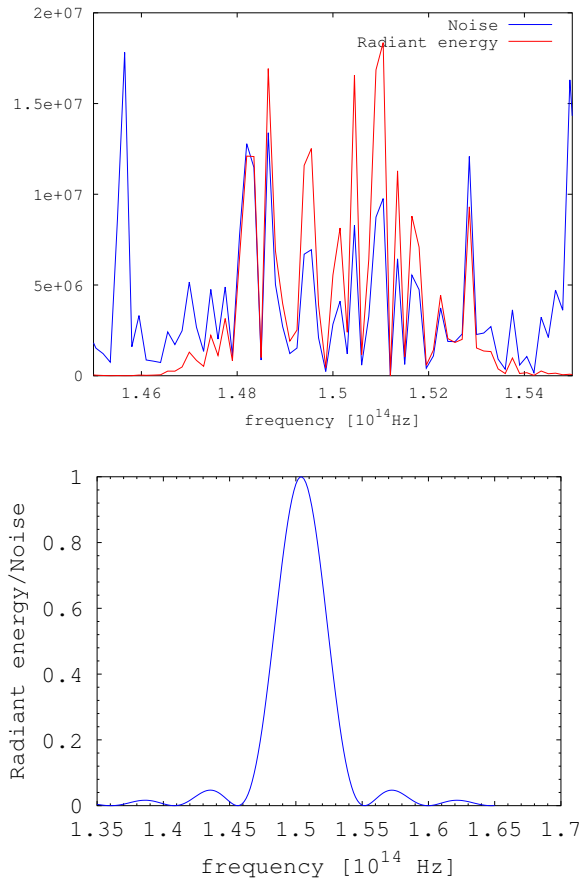

Figure 5: (a) Current noise spectrum of a random cold beam with Poissonian distribution (shot-noise) and the corresponding UR spectrum on-axis for the same electron distribution (same realization). The UR spectrum spikes are correlated to the current noise spikes. (b) The ratio of the UR to current noise for the same beam realization shown in (a) replicates sinc$^2(\theta_0 L/2)$ dependence.

between the noise and the radiant energy intensity on axis, but reveals significant deviation off-axis due to 3D effect.

CONCLUSIONS

In this paper we presented formulation and numerical analysis of controlled suppression/enhancement of spontaneous emission of Undulator Radiation from a correlated electron beam. The electron correlation in the beam is established and controlled by propagating the beam through a drift section followed by a dispersive section (Chicane). The beam drift is simulated by a 3D code (GPT) that takes into account space charge interactions (Coulomb interaction between particles). The collective undulator radiation radiant intensity and spectral radiant intensity are calculated in the far diffraction zone by coherent summation of the wave packet fields emitted by the individual electrons and modeled by analytic expressions taking into account all 3D effects, including longitudinal and transverse correlation, e-beam spread and off-axis radiation emission. The 3D simulations

ISBN 978-3-95450-134-2

are motivated by observation of 3D effects in emission of correlated beam UR (both suppression and enhancement) that were measured in a recent experiment that we presented earlier [1]. At present, we applied the simulations to an arbitrary example of an undulator of 10 periods $\lambda_w = 15.4\,\mathrm{cm}$ operating with a 100 MeV cold e-beam of radius $r_b = 1\,\mathrm{mm}$, emitting UR of central wavelength $\lambda = 2\,\mu\mathrm{m}$ on axis. The drift section simulation was done for the same beam parameters for a drift length $L_d = 10\,\mathrm{m}$ that corresponds to plasma oscillation phase of $\phi_p = \pi/6$. The simulations demonstrate the presence of 3D effects of transverse correlation, that are usually not taken into consideration. However, they do not really simulate the experiment of [1] that was conducted with different parameters.

REFERENCES

[1] D. Ratner et al., PRST - ACCELERATORS AND BEAMS 18, 050703 (2015)

[2] E. Allaria et al., Nat. Photonics 7, 913 (2013)

[3] M. Labat et al., "High-Gain Harmonic-Generation Free-Electron Laser Seeded by Harmonics Generated in Gas", Phys. Rev. Lett., 107, 224801 (2011).

[4] A. Marinelli et al., Phys. Rev. Lett. 110, 264802 (2013)

[5] Z. Huang, J. Wu and T. Shaftan, "Microbunching Instability due to Bunch Compression", SLAC-PUB-1159, (December, 2005)

[6] H. Haus and N. Robinson, "The minimum noise figure of microwave beam amplifiers", Proc. IRE 43, 981 (1955).

[7] A. Gover and E. Dyunin, "Collective-Interaction Control and Reduction of Optical Frequency Shot Noise in Charged-Particle Beams", PRL 102, 154801, (2009).

[8] A. Marinelli and J. Rosenzweig, "Microscopic kinetic analysis of space-charge induced optical microbunching in a relativistic electron beam", Phys. Rev. ST Accel. Beams, 13, 110703 (2010).

[9] K.-J. Kim, in Proceedings of the 2011 FEL Conference (2011).

[10] D. Ratner, Z. Huang and G. Stupakov, "Analysis of shot noise suppression for electron beams", Phys. Rev. ST-AB 14, 060710 (2011).

[11] A. Gover, T. Duchovni, E. Dyunin, and A. Nause, "Collective microdynamics and noise suppression in dispersive electron beam transport", Physics of Plasmas, 18 (2011).

[12] A. Gover and E. Dyunin, Journal of Quantum Electronics 132166 (2010).

[13] A. Gover, A. Nause, E. Dyunin, and M. Fedurin, "Beating the shot-noise limit", Nature Physics, 8, 877 (2012).

[14] D. Ratner and G. Stupakov, "Observation of shot noise suppression at optical wavelengths in a relativistic electron beam", Phys. Rev. Lett., 109, 034801 (2012).

[15] A. Nause, E. Dyunin, and A. Gover, "Short wavelength limits of current shot-noise suppression", Phys. Plasmas 21, 083114 (2014) ; Erratum: Phys. Plasmas 21, 129904 (2014)

[16] A. Gover, "Superradiant and stimulated-superradiant emission in prebunched electron-beam radiators. I. Formulation", Phys. Rev. Special Topics - Accelerators and Beams 8, 030701 (2005)

[17] A. Nause, E. Dyunin and A. Gover, "Optical frequency shot-noise suppression in electron beams: Three-dimensional analysis", Jour. Appl. Phys. 107, 103101 (2010).

[18] M. Venturini, Phys. Rev. ST Accel. Beams 11, 034401

[19] R. Ianconescu, "Radiation from charges in the continuum limit" , AIP Advances, 3 (6), (2013).

ISBN 978-3-95450-134-2